Eur. Phys. J. Appl. Phys. **55**, 23902 (2011)
DOI: 10.1051/epjap/2011100428

THE EUROPEAN PHYSICAL JOURNAL APPLIED PHYSICS

Regular Article

Determination of critical island size in *para*-sexiphenyl islands on SiO_2 using capture-zone scaling

S. Lorbek[1], G. Hlawacek[1,2], and C. Teichert[1,a]

[1] Institute of Physics, University of Leoben, Franz Josef Strasse 18, 8700 Leoben, Austria
[2] Physics of Interfaces and Nanomaterials, MESA+ Institute for Nanotechnology, University of Twente, P.O. Box 217, 7500 AE Enschede, The Netherlands

Received: 22 October 2010 / Accepted: 26 May 2011
Published online: 11 August 2011 –

Abstract. One of the important parameters in understanding the mechanism of the early stage of organic thin-film growth is the critical nucleus size i^*. Here, submonolayer films of *para*-sexiphenyl grown on amorphous silicon dioxide substrates were investigated by means of atomic-force microscopy and have been analyzed using the recently proposed capture-zone scaling. Applying the generalized Wigner surmise we determine from the capture-zone distribution i^* at room temperature and 373 K. The results are compared to traditional analysis by island-size scaling and the applicability of the capture-zone scaling is critically discussed with respect to island shape.

1 Introduction

In the last three decades, significant progress has been made in developing organic semiconductor molecules and applying them in organic electronics [1]. Nevertheless, the basics in thin-film growth of organic molecules are not yet fully understood. Especially, knowledge of the initial nucleation process during deposition of conjugated molecules will be crucial for the design of growth routes resulting in smooth films of defined molecular orientation. Such films are a prerequisite for the fabrication of electronic devices like organic light-emitting diodes (OLED), solar cells, and organic field effect transistors (OFET) [2–5].

This work deals with the island nucleation of the model molecule *para*-sexiphenyl (6P) deposited on Si(0 0 1) wafers covered by native oxide. 6P – schematically presented in Figure 1 – is a rod-like oligophenylene molecule ($C_{36}H_{26}$) with a length of 2.7 nm. Films formed from lying 6P molecules – i.e., with their long molecular axis parallel to the surface – have been shown to be a good candidate for high-performance blue light-emitting diodes [6]. Furthermore, blue lasing has been demonstrated from such self-organized nanostructured 6P aggregates [7]. 6P also features a relatively high charge carrier mobility, and thus films of upright standing molecules are tailor made for OFET applications.

One crucial parameter to describe the process of nucleation in the early stage of crystalline film growth is the critical nucleus size i^*. It describes a nucleus which still has a significant probability to decay at the given growth temperature and deposition rate [8]. Or conversely, $i^* + 1$ is the smallest number of atoms or molecules that will form a stable nucleus. The first procedure to determine i^* from growth experiments was developed by Venables in the 1970s [9]. There, samples which were grown at different deposition rates in the aggregation regime were analyzed. In this regime, the island density remains constant and only the mean island size increases. In the 1990s, a different approach was suggested by Amar and Family using a general scaling function which was fitted to a distribution of island sizes for the determination of i^* [10,11]. Both procedures have been applied to atomic systems quite successfully. However, Venables' procedure requires a sequence of samples grown at different growth rates, while all other parameters remain unchanged.

Recently, capture-zone scaling (CZS), based on the generalized Wigner surmise (GWS), was proposed as a method to obtain i^* [12,13]. This method relies on the calculation of Wigner-Seitz cells surrounding each nucleation center, utilizing Voronoi tessellation, which was proposed earlier by Mulheran and Blackman as a way to characterize the capture zone of a growing island [14,15]. Experimental work [15–19], especially from the field of organic semiconductor thin-film growth, demonstrates the applicability of this method. The virtue of it – comparing with Venables' approach – is based on the fact that only one growth experiment is necessary to obtain i^* for a given temperature. Here, we apply this approach to determine i^* for the growth of *para*-sexiphenyl on an amorphous silicon oxide substrate at two different growth temperatures.

[a] e-mail: teichert@unileoben.ac.at

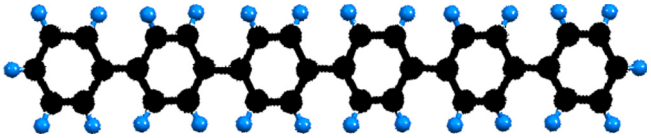

Fig. 1. (Color online) Scheme of a 6P molecule ($C_{36}H_{26}$). It comprises six phenyl rings single bonded in a linear fashion.

The resulting data are critically evaluated by comparison to the values obtained by island-size scaling (ISS) proposed by Amar and Family. For room temperature growth, resulting in rather compact islands with a fractal dimension d of about 2, both procedures yield an i^* of 1 where CZS yields the more reliable fit. For 373 K, where ramified islands ($d = 1.75$) are obtained, CZS is found to be not applicable. Thus, the i^* value of 2 – obtained by ISS – has been taken.

2 Experimental and analytical methods

The growth experiments were performed using organic molecular beam epitaxy (OMBE) in an ultra-high vacuum (UHV) chamber with a base pressure better than 10^{-9} mbar. Si(0 0 1) substrates covered with a native oxide were cleaned by annealing at 780 K with a homemade electron bombardment heater for 900 s. To minimize sample recontamination, evaporation on these amorphous substrates has been started directly after cooling down. The selected growth temperatures were 300 K (RT) and 373 K. Utilizing quartz crystal microbalance measurements, for both experiments a 6P film with a nominal thickness of 0.3 nm has been deposited. This corresponds to a surface coverage of 12% assuming monolayer high islands (2.6 nm) of almost upright standing molecules.

Atomic-force microscopy (AFM) in tapping mode has been used under ambient conditions to characterize the resulting film morphology. A Digital Instruments Multimode AFM with a Nanoscope IIIa controller and standard silicon AFM cantilevers were employed. The AFM probes used had a typical resonance frequency of 300 kHz and their tips' half cone opening angle was 10°.

Capture-zone areas A have been determined from appropriate AFM images using Voronoi tessellation. After excluding polygons which possess vertices outside the image, normalization was performed to obtain the fluctuating variable

$$s \equiv A/\langle A \rangle. \tag{1}$$

Histograms of s values have been obtained using an optimal bin size

$$\nu = 3.49\sigma N^{-1/3}, \tag{2}$$

where N is the number of data points and σ is the standard deviation of all s [20]. The distribution function of the GWS [12]

$$P_\beta(s) = a_\beta s^\beta \mathrm{e}^{-b_\beta s^2} \tag{3}$$

was then fitted to the histogram using the method of least squares with the Levenberg-Marquardt algorithm. The parameters a_β and b_β have the following form:

$$a_\beta = 2\Gamma\left(\frac{\beta+2}{2}\right)^{\beta+1} \Big/ \Gamma\left(\frac{\beta+1}{2}\right)^{\beta+2}, \tag{4}$$

and

$$b_\beta = \left[\Gamma\left(\frac{\beta+2}{2}\right) \Big/ \Gamma\left(\frac{\beta+1}{2}\right)\right]^2. \tag{5}$$

For the two-dimensional case, the only parameter in the function, β, corresponds to $i^* + 2$ [13,21,22].

In addition, the method of Amar and Family [10] has been used to obtain i^*. The island-size distribution (ISD), corresponding to the island size $\tilde{s}$ at a coverage θ,

$$N_{\tilde{s}}(\theta) = \theta \tilde{S}^{-2} f_{i^*}(\tilde{s}/\tilde{S}) \tag{6}$$

with the average island size $\tilde{S}$ and the scaled ISD $f_{i^*}(\tilde{s}/\tilde{S})$ leads to a histogram which was compared to the following general scaling form of the ISD for different $i^* \geq 1$:

$$f_{i^*}(u) = C_{i^*} u^{i^*} \mathrm{e}^{-i^* a_{i^*} u^{1/a_{i^*}}}, \tag{7}$$

where $u = \tilde{s}/\tilde{S}$. The values of the constants C_{i^*} and a_{i^*} for each i^* emerge from the implicit geometrical equations

$$\Gamma\left[(i^*+2)a_{i^*}\right] / \Gamma\left[(i^*+1)a_{i^*}\right] = (i^* a_{i^*})^{a_{i^*}}, \tag{8}$$

and

$$C_{i^*} = (i^* a_{i^*})^{(i^*+1)a_{i^*}} \Big/ a_{i^*} \Gamma\left[(i^*+1)a_{i^*}\right]. \tag{9}$$

In principle, the statistics are slightly better when analyzing the ISD as compared to the situation for the Voronoi tessellation because islands near the image border have to be ignored for the tessellation but might be included in the ISD. For both cases the critical nucleus size i^* has been determined by selecting the value that yields the highest coefficient of determination R^2 with the sample data.

3 Results and discussion

In Figure 2, the results of our AFM-based morphological analysis are presented for a 6P film grown at RT in the aggregation regime. The typical morphology is shown in Figure 2a. Figure 2c shows a high-resolution AFM image of a single island. The islands are irregularly shaped with a mean lateral diameter of about 500 nm. In fact, a quantitative measure for the island shape is the fractal dimension d [23]. Using the box-counting method, we obtain at RT an average fractal dimension d of 1.98. The height profile indicated by a red line in Figure 2c is shown in Figure 2d. From the island height of 2.6 nm we conclude that the molecules are standing nearly upright on the substrate. It is noticeable that about 50% of the islands exhibit already a second layer island of the same height. This is due to the presence of an effective Ehrlich-Schwoebel barrier [24,25] for interlayer mass transport as has been recently studied in detail for 6P films on ion bombarded mica substrates [26]. Different from the latter case, where the first layer molecules are significantly tilted

https://doi.org/10.1051/epjap/2011100428 Published online by Cambridge University Press

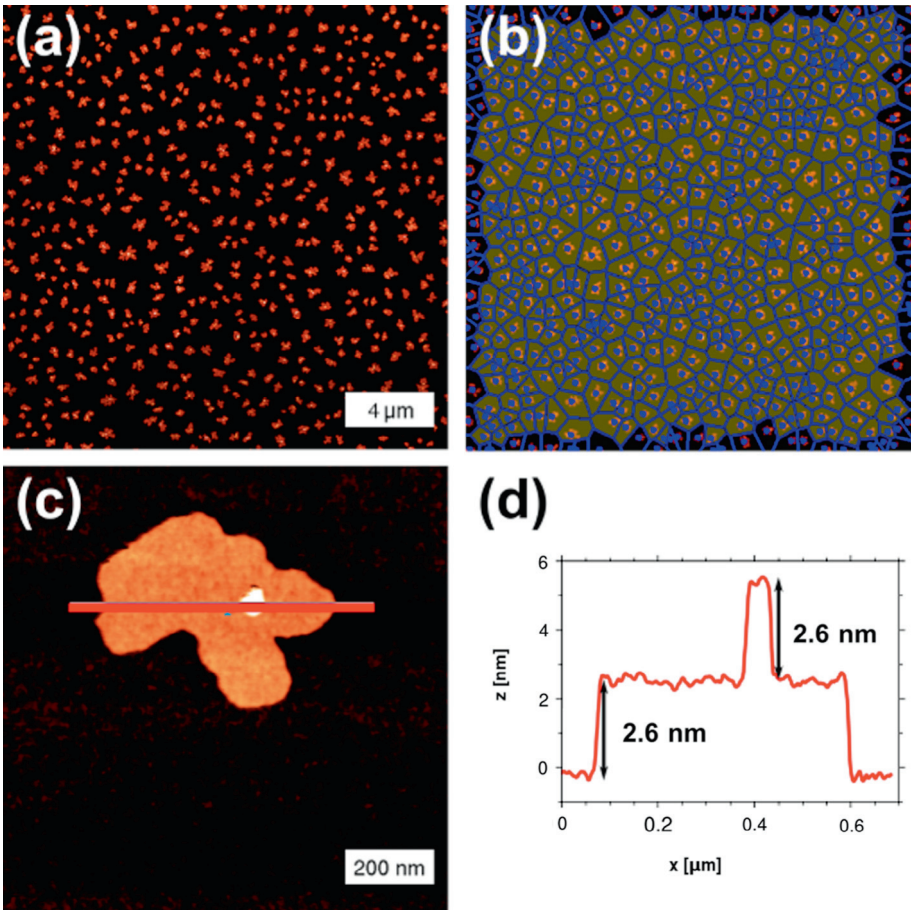

Fig. 2. (Color online) (a) $20 \times 20\,\mu m^2$ AFM image of a sample grown at RT with a z-scale of 5 nm. (b) Image masked with the calculated Voronoi polygons. (c) $1 \times 1\,\mu m^2$ AFM image of a single island. (d) Corresponding height profile represented by the red line in (c).

toward the substrate, we observe here a substantial second layer formation already in the aggregation stage, related to the smaller tilt angle of the molecules [26].

The Voronoi tessellation used to obtain the capture zones is presented in Figure 2b. In total, seven such $20 \times 20\,\mu m^2$ large Voronoi tessellations from different sample positions have been used to build the histogram of capture-zone areas shown in Figure 3. GWS distributions for several values of i^* have been added to the diagram. The best least square fit, accentuated by a thicker line, yields an i^* of 1, i.e., two molecules will form a stable nucleus.

Figure 4 shows the histogram of the island sizes obtained from the same set of images. To allow for a direct comparison to CZS, islands on the image rim have been excluded and thus an identical set of islands has been used for analysis. A selection of ISDs is also plotted. A least square fit of i^* to the data yields a value of 1.50 (dashed line), indicating that the stable nucleus has to be formed by either two or three molecules. This is in good agreement with the result of i^* equal to 1 obtained by CZS. However, we have to note that the CZS analysis yields the better R^2 coefficients which we address to the following: According to the different mathematical nature of GWS in equation (3) and the scaling form in equation (7), the fit of i^* in the GWS has a better correlation with the asymmetric data set than the more symmetric scaling function of Amar and Family. This was already mentioned by Pimpinelli and Einstein [12,13].

Corresponding AFM results for the case of 6P deposition at 373 K are presented in Figure 5. Here, the island density is dramatically reduced and the average lateral island size is about 5 μm for the same coverage. This is in agreement with classical nucleation theory which predicts for a higher substrate temperature a smaller number of nucleation events owing to the increased mobility of 6P on the substrate surface. As is evident from Figure 5c, also the island shape changes significantly with increasing growth temperature. At this elevated temperature, the islands are ramified. Compared to room temperature growth, the fractal dimension d decreases to a value of 1.75. This observation seems to contradict classical nucleation theory, but has been observed earlier by another group for the same system [27]. The measured island height (Fig. 5d) is again an indication for upright standing molecules. Thirteen $85 \times 85\,\mu m^2$ AFM images had to be analyzed to observe at least 250 nucleation events suitable for Voronoi tessellation which is a minimum for a

https://doi.org/10.1051/epjap/2011100428 Published online by Cambridge University Press

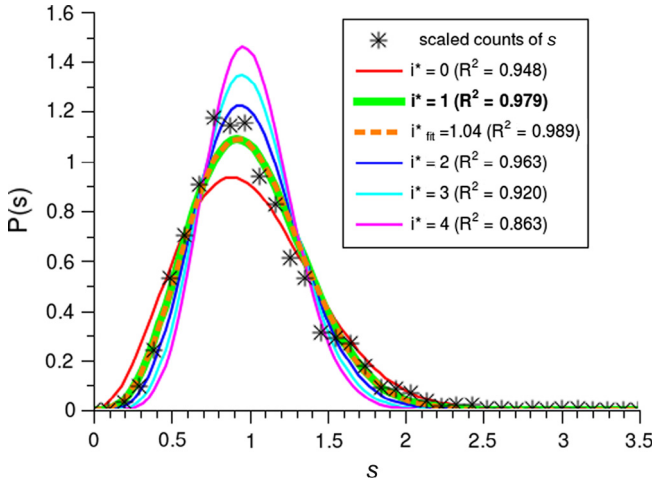

Fig. 3. (Color online) Capture-zone histogram obtained from the sample grown at RT. About 2700 capture-zone areas were analyzed. Capture-zone distributions for several values of i^* are plotted for comparison. The dashed line is a least square fit to the data of the histogram. The thick line marks the selected i^*.

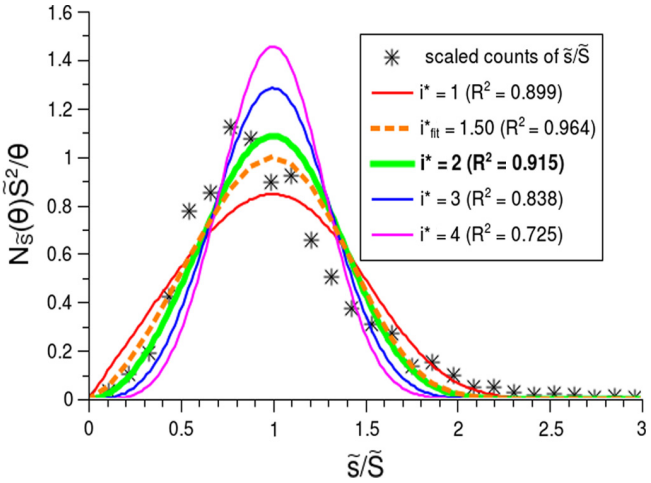

Fig. 4. (Color online) Island-size histogram obtained from the sample grown at RT. The same data set of about 2700 islands was analyzed by the model of Amar-Family [10] and overlaid by fits for several i^*. The dashed line is a least square fit to the data of the histogram. The thick line marks the selected i^*.

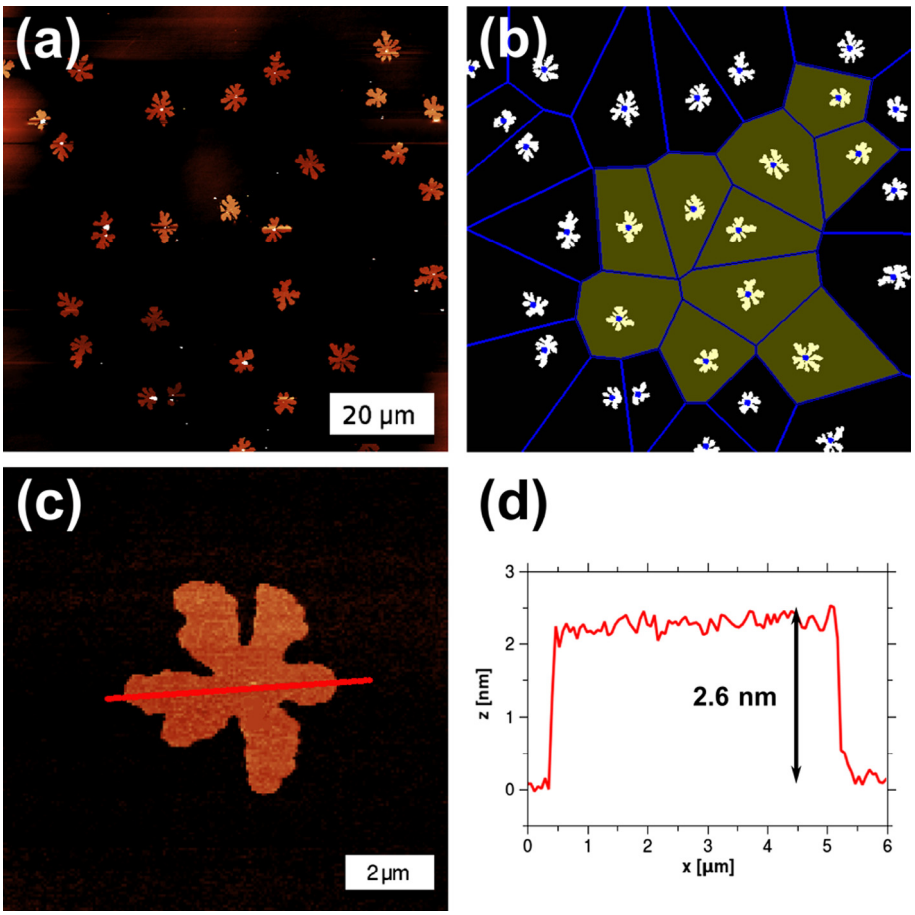

Fig. 5. (Color online) (a) $85 \times 85\,\mu m^2$ AFM image of a sample grown at 373 K with a z-scale of 5 nm. (b) Image masked with the calculated Voronoi polygons (yellow areas mark the used ones). (c) $10 \times 10\,\mu m^2$ AFM image of a single island. (d) Corresponding height profile represented by the red line in (c).

https://doi.org/10.1051/epjap/2011100428 Published online by Cambridge University Press

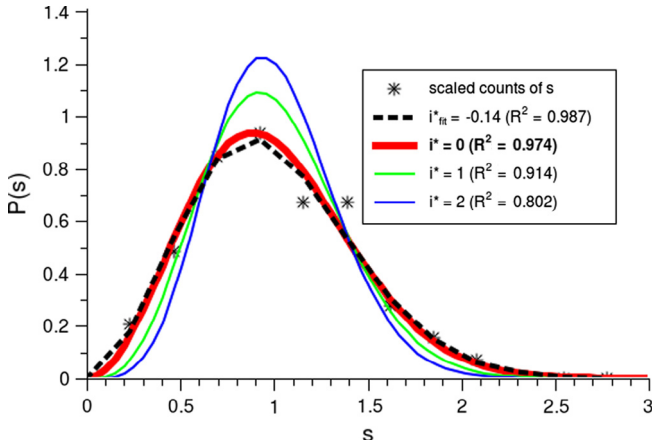

Fig. 6. (Color online) Capture-zone histogram obtained from the sample grown at 373 K. Here, about 250 capture-zone areas were analyzed and supplemented with the CZD for several values of i^* for comparison. The dashed line is a least square fit to the data of the histogram. The thick line marks the selected i^*.

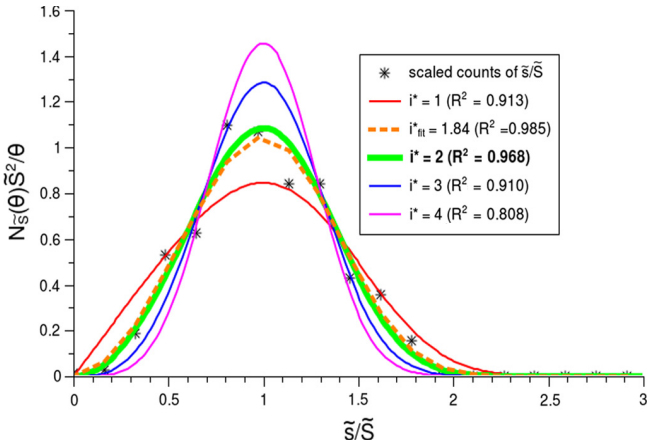

Fig. 7. (Color online) Island-size histogram from the sample grown at 373 K. About 430 islands were analyzed by the model of ISD [10] and supplemented with the ISD for several values of i^* for comparison. The dashed line is a least square fit to the data of the histogram. The thick line marks the selected i^*.

statistically sound histogram (Fig. 6). The best fit – with a reasonable R^2 value of 0.97 – is obtained for i^* equal to 0. In other words, at 373 K one 6P molecule seems to form a stable nucleus which is a rather suspicious result. However, the analysis of this sample using the island-size model (Fig. 7) yields an i^* of 2, where the statistics became slightly better because nearly 200 more islands from the image rims could be taken into account.

Possible reason for the discrepancy between the two methods when applied to ramified islands will be discussed next. Mulheran and Blackman [14] pointed out that a Voronoi tessellation for obtaining the capture zone will overestimate the size of small islands and underestimate it for large ones. In addition, the capture-zone boundaries are more likely equidistant from the edges of neighboring islands and not their centers. Popescu et al. [28] have shown that the mean-field distributions of dendritic islands have sharp peaks and diverge because of their dependence on coverage. Pimpinelli and Einstein [12,13] postulated no dependence of their GWS on the coverage. From their mean-field argument they directly derive the shape of $P(s)$ and thus β. For the case of ramified islands the mean-field assumption is most likely not true and CZS using the GWS yields unreliable results. Therefore, we assume that i^* at 373 K is 2 (following the ISS) and thus by one molecule larger than for room temperature growth. However, for our RT experiment where compact islands are observed, CZS yields better results than ISS. An advantage of CZS is that it is less dependent on the exact island size and thus shape, as only the center of mass is required. Consequently, smaller magnification is necessary and reasonable statistical quality is reached more easily.

4 Conclusions

We have applied capture-zone scaling using the generalized Wigner surmise [12,13] to obtain the critical nucleus size for 6P islands grown on amorphous SiO_2 at two different substrate temperatures. According to our findings, for room temperature the stable nucleus is formed of two molecules, in good agreement with island-size scaling analysis following Amar and Family [10]. As we have shown elsewhere [29], i^* values of compact islands obtained using GWS are not only in good agreement with results from ISS but also with those from rate equation [9]. However, the applicability of CZS to ramified islands should be critically reviewed on a case-to-case basis as the mean-field approach might be violated for some extreme island shapes as we demonstrated for the growth of ramified 6P islands on SiO_2 at 373 K. In the latter case, CZS failed and i^* value of 2 has been taken from ISS analysis.

In general, for compact islands CZS is advantageous over rate equation approaches since only a single experiment is necessary. Compared to ISS, images with a lower resolution are sufficient to obtain the center of mass with the required accuracy. Further the GWS distribution fits better the experimentally determined data than the more symmetric scaling function in the ISS analysis.

In the current stage, we do not know whether the stable nuclei are already composed of upright standing molecules as found for the larger islands analyzed here. For the future, molecular dynamic simulations are planned to reveal the details of the molecule erection.

This work has been funded by the Austrian Science Fund (FWF) under Project #S9707-N20. Further, we would like to acknowledge stimulating discussions by A. Winkler and M. Kratzer.

References

1. C.K. Chiang, C.R. Fincher, Y.W. Park, A.J. Heeger, H. Shirakawa, E.J. Louis, S.C. Gau, A.G. MacDiarmid, Phys. Rev. Lett. **39**, 1098 (1977)
2. U. Mitschke, P. Bäuerle, J. Mater. Chem. **10**, 1471 (2000)

https://doi.org/10.1051/epjap/2011100428 Published online by Cambridge University Press

3. H. Hoppe, N.S. Sariciftci, J. Mater. Res. **19**, 1924 (2004)
4. J.-O. Vogel, I. Salzmann, S. Duhm, M. Oehzelt, J.P. Rabe, N. Koch, J. Mater. Chem. **20**, 4055 (2010)
5. T.B. Singh, G. Hernandez-Sosa, H. Neugebauer, A. Andreev, H. Sitter, N.S. Sariciftci, Phys. Stat. Sol. B **243**, 3329 (2006)
6. H. Yanagi, T. Morikawa, Appl. Phys. Lett. **75**, 187 (1999)
7. A. Andreev, F. Quochi, F. Cordella, A. Mura, G. Bongiovanni, H. Sitter, G. Hlawacek, C. Teichert, N.S. Sariciftci, J. Appl. Phys. **99**, 034305 (2006)
8. I.V. Markov, *Crystal Growth for Beginners*, 2nd edn. (World Scientific Publishing, Singapore, 2003)
9. J.A. Venables, Philos. Mag. **27**, 697 (1973)
10. J.G. Amar, F. Family, Phys. Rev. Lett. **74**, 2066 (1995)
11. R. Ruiz, B. Nickel, N. Koch, L.C. Feldman, R.F. Haglund Jr., A. Kahn, F. Family, G. Scoles, Phys. Rev. Lett. **91**, 136102 (2003)
12. A. Pimpinelli, T.L. Einstein, Phys. Rev. Lett. **99**, 226102 (2007)
13. A. Pimpinelli, T.L. Einstein, Phys. Rev. Lett. **104**, 149602 (2010)
14. P.A. Mulheran, J.A. Blackman, Phys. Rev. B **53**, 10261 (1996)
15. M. Brinkmann, S. Graff, F. Biscarini, Phys. Rev. B **66**, 165430 (2002)
16. S. Miyamoto, O. Moutanabir, E.E. Haller, K.M. Itho, Phys. Rev. B **79**, 165415 (2009)
17. M. Brinkmann, S. Pratontep, C. Contal, Surf. Sci. **600**, 4712 (2006)
18. B.R. Conrad, E. Gomar-Nadal, W.G. Cullen, A. Pimpinelli, T.L. Einstein, E.D. Williams, Phys. Rev. B **77**, 205328 (2008)
19. A.B.H. Hamouda, T.J. Stasevich, A. Pimpinelli, T.L. Einstein, J. Phys. Cond. Mat. **21**, 084215 (2009)
20. D.W. Scott, Biometrika **66**, 605 (1979)
21. M. Li, Y. Han, J.W. Evans, Phys. Rev. Lett. **104**, 149601 (2010)
22. F. Shi, Y. Shim, J.G. Amar, Phys. Rev. E **79**, 011602 (2009)
23. P. Meakin, *Fractals, Scaling and Growth Far From Equilibrium* (University Press, Cambridge, 1998)
24. G. Ehrlich, F. Hudda, J. Chem. Phys. **44**, 1039 (1966)
25. R.L. Schwoebel, E.J. Shipsey, J. Appl. Phys. **37**, 3682 (1966)
26. G. Hlawacek, P. Puschnig, P. Frank, A. Winkler, C. Ambrosch-Draxl, C. Teichert, Science **321**, 108 (2008)
27. J. Yang, T. Wang, H. Wang, F. Zhu, G. Li, D. Yan, J. Chem. B **112**, 7816, 7821 (2008)
28. M.N. Popescu, J.G. Amar, F. Family, Phys. Rev. B **64**, 205404 (2001)
29. T. Potocar, S. Lorbek, D. Nabok, Q. Shen, L. Tumbek, G. Hlawacek, P. Puschnig, C. Ambrosch-Draxl, C. Teichert, A. Winkler, Phys. Rev. B **83**, 075423 (2011)

https://doi.org/10.1051/epjap/2011100428 Published online by Cambridge University Press